

Received September 24, 2020, accepted October 14, 2020, date of publication October 19, 2020, date of current version October 29, 2020.

Digital Object Identifier 10.1109/ACCESS.2020.3032038

An Optimized Parameter Design Method for Passivity-Based Control in a *LCL*-Filtered Grid-Connected Inverter

FABAN ZHENG¹, WEIMIN WU¹, (Member, IEEE), BOLIN CHEN¹, (Member, IEEE),
AND EFTICHIOS KOUTROULIS², (Senior Member, IEEE)

¹Department of Electronic Engineering, Shanghai Maritime University, Shanghai 201306, China

²School of Electrical and Computer Engineering, Technical University of Crete, 731 00 Chania, Greece

Corresponding author: Weimin Wu (wmwu@shmtu.edu.cn)

This work was supported in part by the National Natural Science Foundation of China under Grant 51877130, in part by the National Key Research and Development Project of China under Grant 2017YFGH001164, and in part by the Project performed within the framework of the eSOLAR: Principle and Control of High-Efficiency Buck-Boost Type Photovoltaic Inverter Project of the Program Bilateral and Multilateral Research and Technology co-operation between Greece and China funded by the Operational Program Competitiveness, Entrepreneurship and Innovation 2014–2020 (co-funded by the European Regional Development Fund) and managed by the General Secretariat of Research and Technology, Ministry of Education, Research, and Religious Affairs, Greece, under Project eSOLAR/T7ΔKI-00066.

ABSTRACT Nowadays, the Passivity-Based Control (PBC) has been successfully applied to digitally controlled Grid-Connected Inverter (GCI) with *LCL* filter. As a nonlinear method, the PBC controller has strong robustness against the parameter drift of the *LCL* filter and the grid impedance, where the parameters of the PBC controller still need to be designed carefully to achieve a good control performance. The existing design methods are based on separating the PBC controller into three control loops. Therefore, the design process is cumbersome, especially for inexperienced engineers, due to the complex structure of the PBC controller. In this article, an intelligent Particle Swarm Optimization (PSO) algorithm is utilized to simplify the parameters design of the PBC controller, where the difficulty of manual calculations is avoided and the parameters can be more easily and efficiently obtained using MATLAB in offline mode. Furthermore, a Kalman filter observer is adopted to estimate the state variables in the PBC controller, where only the grid-injected current needs to be sampled in the overall GCI system. Simulations and experiments are provided to verify the correctness and effectiveness of the proposed PBC controller design method.

INDEX TERMS Grid-connected inverter, Kalman filter, *LCL* filter, passivity-based control, particle swarm optimization.

I. INTRODUCTION

With the concern of the environment, the renewable energy has attracted more and more attentions. The Grid-Connected Inverter (GCI) is an important interface unit inserted between renewable energy and the grid [1], where a power filter, such as *L*, *LC*, and *LCL*, is also indispensable to suppress the harmonic current generated by the high frequency switching. Compared with the *L* and *LC* filter, the *LCL* filter is often utilized in industry, owing to its better harmonic attenuation performance and lower cost [2], [3].

To achieve the excellent control performance of *LCL* filtered GCI, PI-Based Control [4] and Proportional-Resonance Control [5], [6] are commonly adopted as linear controllers,

The associate editor coordinating the review of this manuscript and approving it for publication was Elisabetta Tedeschi.

providing the high control gain and tracking the reference without steady-state error. However, the whole system often suffers from the resonance, which may seriously deteriorate its stability. In order to suppress the possible resonance, passive or active damping methods have been widely adopted [7]–[9]. Note that the damping methods can effectively ensure the stability of system, but at extra costs. For example, the passive damping consumes the extra power of the system, while the active damping increases the numbers of sensors.

Nowadays, owing to the more and more powerful processors with the high computational capacity, many nonlinear control strategies, such as Predictive Control [10]–[12], Slide Model Control [13], [14], Adaptive Control [15], [16] and Passivity-Based Control (PBC) [17], [18] have been applied to GCI. Among the nonlinear control strategies, the PBC has

strong robustness against external perturbations and parameter variations. The stability of the GCI/electric-grid interconnection is ensured, by rendering the system to be passive [19]. The PBC has attracted considerable interests from many scholars.

It is worth noting that the passivity theory is also adopted by linear controllers [20], where the *LCL*-filtered GCI with linear controllers is equivalent to an admittance model and the stability of the system is analyzed by the frequency-domain passivity theory. Although this method is different from the PBC controller design approach based on Euler–Lagrange (EL) model in this paper, it is a good method for analyzing system stability.

In [21], a PBC controller with three control loops was proposed, which guaranteed high-quality the grid-injected current and had strong robustness against system parameter changes and external perturbations. As an important factor, the damping gains of the PBC controller determine the control performance. However, the appropriate damping gains are very difficult to find due to the complex structure of the PBC controller. In practical applications, the trial-and-error method is often adopted. In [18], a step-by-step parameters design method was proposed to select the damping gains of PBC controller, where the three control loops are separated from inside to outside and the inherent steady-state error of grid-injected current is effectively limited. Although the damping gains designed by this method provide good steady-state performance and guarantee robustness against parameter variations, the design process of this method is a little cumbersome.

The artificial intelligence techniques have been improved significantly during the last years. Among them, the Particle Swarm Optimization (PSO) algorithm is gradually adopted to design the parameters of controllers, due to its flexibility, simplicity and ease of use. In [22], the PSO algorithm was employed to search for the optimal settings of operating parameters of PI controllers, filter, and power sharing coefficients such that satisfactory system performance is achieved under different disturbances. In [23], the weighting matrix for the LQR was optimized using the PSO algorithm, which made the tuning procedure simpler in comparison to the often reported trial-and-error method for determining the weighting matrix. The automated parameter-search method by PSO algorithm ignores the complex structure of the controller and obtains the optimal parameters by continuously updating the fitness function [24]. In order to assist the design of PBC controller, the PSO algorithm will be applied to select the parameters in this article.

In addition, the PBC controller is similar to the full-state feedback control [25], which needs to sample multiple state variables, including inverter-side current, capacitor voltage, grid-injected current and Point of Common Coupling (PCC) voltage. In order to reduce the number of sensors, an observer is required. In [18], [26], a state observer was adopted to estimate state variables, where the values of inverter-side current and capacitor voltage can be observed. Note that, in [27],

a Kalman filter observer had been utilized together with only one current sensor, which achieved a good performance of the controller with a low total harmonic current distortion (THD).

In this article, an improved PBC controller combining the PSO algorithm and a Kalman filter observer are proposed for the three-phase *LCL*-filtered GCI. Compared to the past-proposed control methods for *LCL*-filtered GCI, the design technique proposed in this article exhibits the following novelty: (i) the parameters design of the PBC controller is optimized by the PSO algorithm to achieve the required transient and steady-state performance of the overall GCI system and (ii) the PBC controller can be implemented with only grid-injected current sensors.

The rest of this article is organized as follows. The mathematical model and conventional PBC controller of the *LCL*-filtered three-phase GCI will be presented in Section II. Then, in Section III, an improved PBC controller based on the PSO algorithm and a Kalman filter observer are proposed, where optimized parameters of proposed PBC controller can be easily obtained by applying the PSO algorithm, while, additionally, the required number of sensors is reduced by employing a Kalman filter observer. The effectiveness of the proposed PBC controller is verified by simulation in Section IV. In Section V, the performance of the proposed PBC controller is further demonstrated by a 3-kW experimental device. Finally, the conclusions of the paper are drawn in Section VI.

II. MATHEMATICAL MODEL AND CONVENTIONAL PBC CONTROLLER FOR *LCL*-FILTERED GCI

A. EULER LAGRANGE MODEL OF *LCL*-FILTERED GCI

A full configuration of the GCI with an *LCL* filter and the proposed control structure are shown in Fig. 1, where L_1 , L_2 and C are the inverter-side inductor, the grid-side inductor and the capacitor, respectively; R_1 and R_2 are parasitic resistors; L_g is the equivalent grid inductor; i_1 and i_2 are the inverter-side current and the grid-injected current, respectively; u_{a-b-c} , u_c and v_{pcc} are the inverter output voltage, the capacitor voltage and the PCC voltage, respectively. The driving signal is obtained through Space Vector Pulse Width Modulation (SVPWM) technique. A constant dc-link voltage U_{dc} is assumed, due to that the dc dynamics are quite slow and are reasonably neglected [28].

Based on the two-phase static coordinate α - β , the mathematical equations of an *LCL*-filtered GCI are the following:

$$\begin{cases} L_1 \frac{di_{1\alpha}}{dt} + R_1 i_{1\alpha} + u_{c\alpha} = u_\alpha \\ L_1 \frac{di_{1\beta}}{dt} + R_1 i_{1\beta} + u_{c\beta} = u_\beta \\ C \frac{du_{c\alpha}}{dt} - i_{1\alpha} + i_{2\alpha} = 0 \\ C \frac{du_{c\beta}}{dt} - i_{1\beta} + i_{2\beta} = 0 \\ L_2 \frac{di_{2\alpha}}{dt} + R_2 i_{2\alpha} - u_{c\alpha} = -v_{pcc\alpha} \\ L_2 \frac{di_{2\beta}}{dt} + R_2 i_{2\beta} - u_{c\beta} = -v_{pcc\beta} \end{cases} \quad (1)$$

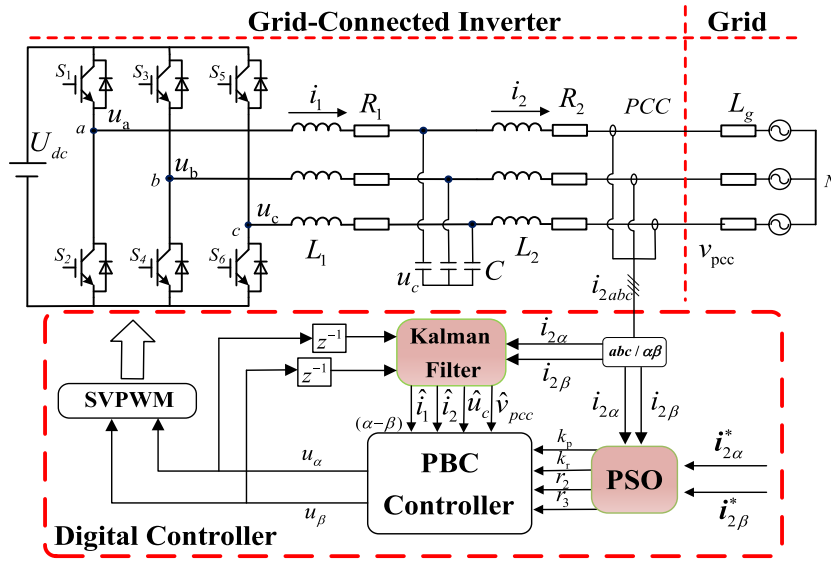


FIGURE 1. Full topology and control structure of Grid-Connected Inverter with LCL filter.

and the state vector are defined as $x = [i_{1\alpha} \ i_{1\beta} \ u_{c\alpha} \ u_{c\beta} \ i_{2\alpha} \ i_{2\beta}]$. In order to exploit the passivity property of LCL-filtered GCI, the mathematical equation (1) is equivalently represented in the Euler Lagrange (EL) model as follows:

$$M\dot{x} + Jx + Rx = u \quad (2)$$

where

$$M = \begin{bmatrix} L_1 & 0 & 0 & 0 & 0 & 0 \\ 0 & L_1 & 0 & 0 & 0 & 0 \\ 0 & 0 & C & 0 & 0 & 0 \\ 0 & 0 & 0 & C & 0 & 0 \\ 0 & 0 & 0 & 0 & L_2 & 0 \\ 0 & 0 & 0 & 0 & 0 & L_2 \end{bmatrix},$$

$$J = \begin{bmatrix} 0 & 0 & 1 & 0 & 0 & 0 \\ 0 & 0 & 0 & 1 & 0 & 0 \\ -1 & 0 & 0 & 0 & 1 & 0 \\ 0 & -1 & 0 & 0 & 0 & 1 \\ 0 & 0 & -1 & 0 & 0 & 0 \\ 0 & 0 & 0 & -1 & 0 & 0 \end{bmatrix},$$

$$R = \begin{bmatrix} R_1 & 0 & 0 & 0 & 0 & 0 \\ 0 & R_1 & 0 & 0 & 0 & 0 \\ 0 & 0 & 0 & 0 & 0 & 0 \\ 0 & 0 & 0 & 0 & 0 & 0 \\ 0 & 0 & 0 & 0 & R_2 & 0 \\ 0 & 0 & 0 & 0 & 0 & R_2 \end{bmatrix},$$

$$u = [u_\alpha \ u_\beta \ 0 \ 0 \ -v_{pcc\alpha} \ -v_{pcc\beta}]^T.$$

B. PASSIVITY OF THE LCL-FILTERED GCI

In order to apply the PBC controller to the LCL-filtered GCI, it is necessary to verify the passivity of the LCL-filtered GCI. The storage energy function of system is defined as

$$H(x) = \frac{1}{2}x^T Mx \quad (3)$$

Then, the time derivative of the storage energy function can be obtained as

$$\dot{H}(x) = x^T M\dot{x} = x^T (u - Jx - Rx) = x^T u - x^T Rx \quad (4)$$

According to the passive theory [29], the equation (4) is transformed into an integral equation as

$$H[x(t)] - H[x(0)] = \int_0^t x^T u dt - \int_0^t x^T Rx dt \quad (5)$$

It can be seen that $\int_0^t x^T u dt$ represents the energy supplied to the system; $\int_0^t x^T Rx dt$ represents the dissipated energy in the system; $H[x(t)] - H[x(0)]$ represents the energy stored inside the system. It denotes that the total energy stored is not higher than the energy supplied. Thus, the LCL-filtered GCI is strictly passive.

C. CONVENTIONAL PBC CONTROLLER

Since the LCL-filtered GCI has been proven to be a passive system, the conventional PBC controller can be deduced as follows.

Firstly, the desired equilibrium points are defined as $x^* = [i_{1\alpha}^* \ i_{1\beta}^* \ u_{c\alpha}^* \ u_{c\beta}^* \ i_{2\alpha}^* \ i_{2\beta}^*]$, and the error vector can be expressed as

$$x_e = x^* - x. \quad (6)$$

Then, by substituting (6) into (2), the error equation can be obtained as

$$M\dot{x}_e + Jx_e + Rx_e = M\dot{x}^* + Jx^* + Rx^* - u. \quad (7)$$

In order to quickly converge x to x^* , the damping $R_d = \text{diag}\{r_3 \ r_3 \ r_2 \ r_2 \ r_1 \ r_1\}$ is added to the error equation, where $r_1, r_2, r_3 > 0$. The error equation (7) is rewritten as

$$M\dot{x}_e + Jx_e + (R + R_d)x_e = M\dot{x}^* + Jx^* + Rx^* + R_dx_e - u. \quad (8)$$

According to (8), the left side of the equation is equal to zero when the error vector x_e tends to zero. Thus, the conventional PBC controller of LCL-filtered GCI can be obtained as

$$u = M\dot{x}^* + Jx^* + Rx^* + R_d x_e. \quad (9)$$

In order to analyze the asymptotic stability, an error energy (Lyapunov) function is defined as

$$H_e(x) = \frac{1}{2} x_e^T M x_e \quad (10)$$

From (8), the left side of the equation can be rewritten as

$$M\dot{x}_e = -Jx_e - (R + R_d) x_e \quad (11)$$

Thus, the time derivative of the error energy function can be obtained as

$$\dot{H}_e(x) = x_e^T M \dot{x}_e = -x_e^T (R + R_d) x_e \quad (12)$$

Since M and $(R + R_d)$ are both positive definite diagonal damping matrices, the conditions of $H_e(x) > 0$, $\dot{H}_e(x^*) = 0$ and $\dot{H}_e(x) < 0$ are satisfied. The error energy function can asymptotically converge to zero, according to the Lyapunov stability criterion [30]. Note that, the damping of R_d determines the convergence rate of $H_e(x)$. A small value of R_d will make the error converge slowly, while a large value may cause system to oscillate. Therefore, a suitable design of the damping of R_d needs to be addressed.

Finally, by expanding (9), the controller is described in detail as follows:

$$\begin{cases} u_\alpha = L_1 \frac{di_{1\alpha}^*}{dt} + R_1 i_{1\alpha}^* + r_3 (i_{1\alpha}^* - i_{1\alpha}) + u_{c\alpha}^* \\ u_\beta = L_1 \frac{di_{1\beta}^*}{dt} + R_1 i_{1\beta}^* + r_3 (i_{1\beta}^* - i_{1\beta}) + u_{c\beta}^* \\ 0 = C \frac{du_{c\alpha}^*}{dt} + r_2 (u_{c\alpha}^* - u_{c\alpha}) + i_{2\alpha}^* - i_{1\alpha}^* \\ 0 = C \frac{du_{c\beta}^*}{dt} + r_2 (u_{c\beta}^* - u_{c\beta}) + i_{2\beta}^* - i_{1\beta}^* \\ -v_{pcc\alpha} = L_2 \frac{di_{2\alpha}^*}{dt} + R_2 i_{2\alpha}^* + r_1 (i_{2\alpha}^* - i_{2\alpha}) - u_{c\alpha}^* \\ -v_{pcc\beta} = L_2 \frac{di_{2\beta}^*}{dt} + R_2 i_{2\beta}^* + r_1 (i_{2\beta}^* - i_{2\beta}) - u_{c\beta}^* \end{cases} \quad (13)$$

The equivalent system diagram of the conventional PBC controller is plotted in Fig. 2, where $e^{-1.5T_s}$ represents $1.5T_s$ time delay associated with the calculation and pulse width modulation (T_s is the inverter sampling period). In order to distinguish control parameters and actual parameters, the parameters (L_1 , L_2 , C) in the controller are marked with subscript “e”. Since the β -axis component has the same structure with the α -axis one, only the α -axis component is shown.

III. PROPOSED PBC CONTROLLER

A. ELIMINATING THE STEADY STATE ERROR

In practical applications, due to disturbances caused by the external environment, the conventional PBC controller may

exhibit a steady-state error. In order to eliminate the steady-state error, many modified PBC methods were adopted, such as the disturbance observer [31], the proportional-integral (PI) regulator [18], [32] and the proportional-resonant (PR) regulator [33] etc. According to [34], it can be known that a PR regulator can better track a sinusoidal current reference than a PI regulator. In this article, a proportional-resonant regulator is employed instead of the damping r_1 of a conventional PBC controller in order to eliminate the steady-state error. The transfer function of the PR regulator is expressed as

$$G_{PR} = k_p + \frac{2k_r s}{s^2 + \omega_0^2} \quad (14)$$

where k_p and k_r are gain coefficients, and ω_0 is the fundamental angular frequency.

B. PARAMETERS DESIGN USING PSO ALGORITHM

From equation (13) and (14), it can be seen that the performance of the PBC controller is determined by the parameters k_p , k_r , r_2 and r_3 . In order to obtain high control performance and convenient design parameters, the PSO algorithm is used to design the parameters of the PBC controller.

The PSO algorithm is an iterative optimization algorithm, which uses a set of particles to find the global minimum of the fitness function in D -dimensional space. Each particle has two characteristics: position P_i , velocity v_i , where i is the i^{th} particle. The position represents the solution of the optimization problem, which is described as $P_i = [p_{i1} \ p_{i2} \ \dots \ p_{id} \ \dots \ p_{iD}]$. The velocity represents the distance that the particle needs to move in each iteration, which is described as $v_i = [v_{i1} \ v_{i2} \ \dots \ v_{id} \ \dots \ v_{iD}]$.

In the process of particle movement, each particle will remember the position where it personally encountered the most fitness. This position with the best fitness $B_i = [b_{i1} \ b_{i2} \ \dots \ b_{id} \ \dots \ b_{iD}]$ is known as the personal best (p_{best}). Moreover, the global best position (g_{best}) $G = [g_1 \ g_2 \ \dots \ g_d \ \dots \ g_D]$ is also obtained by comparing the p_{best} values of entire particle swarm.

In the D -dimensional space, the position and the velocity of the entire particle swarm are updated during each iteration, as follows:

$$\begin{aligned} v_{id}^{n+1} &= wv_{id}^n + \lambda_1 c_1 (b_{id}^n - p_{id}^n) + \lambda_2 c_2 (g_d^n - p_{id}^n) \\ p_{id}^{n+1} &= p_{id}^n + v_{id}^{n+1} \end{aligned} \quad (15)$$

where w is inertial weight; λ_1 and λ_2 are random numbers in the interval $[0, 1]$; c_1 and c_2 are scaling factors that determine the relative relationship of p_{best} and g_{best} ; n is the n^{th} iteration; d is the d^{th} dimension.

The basic idea of the PSO algorithm is that the particles adjust the position and the velocity according to equation (15) in each iteration, while optimal value of each individual's original memory is retained. By comparing the p_{best} and g_{best} of the particle swarm in each iteration, the most fitness of particle is selected. In this article, the position of the particles is represented by the parameters of the controller

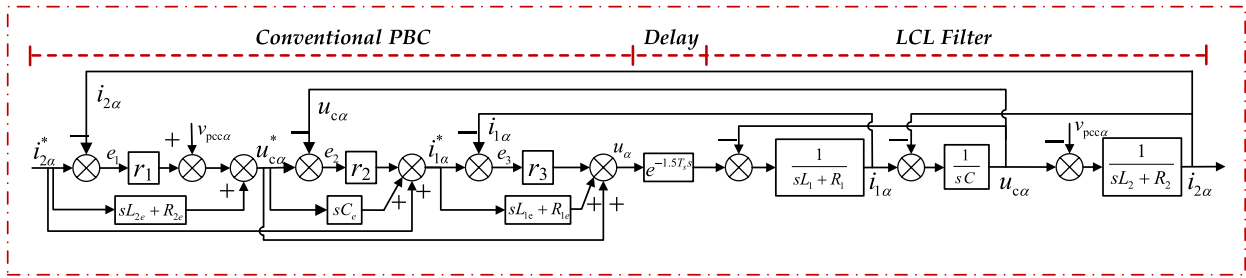


FIGURE 2. Equivalent system diagram of LCL-filtered GCI using the conventional Passivity-Based Controller in S-domain.

(k_p, k_r, r_2 and r_3). The dimension D is determined to be 4 according to the number of parameters. The fitness function is defined as

$$f = \int_0^\infty k_1 t |e_1(t)| + k_2 t |e_2(t)| + k_3 t |e_3(t)| dt \quad (16)$$

where $e_1(t) = i_{2\alpha}^* - i_{2\alpha}$, $e_2(t) = u_{c\alpha}^* - u_{c\alpha}$, $e_3(t) = i_{1\alpha}^* - i_{1\alpha}$; k_1, k_2 and k_3 is the weight coefficient. Since the grid-injected current is used as the important factor in GCI, k_1, k_2 and k_3 of the weight coefficient are set to 0.8, 0.1 and 0.1, respectively.

The flow chart of the PSO algorithm are depicted in Fig. 3. The detailed steps of the PSO algorithm are described as follows:

- 1) The number of particles, the number of iterations, inertial weight w , random numbers λ_1, λ_2 , and scaling factors c_1, c_2 are determined. The position and velocity of each particle are randomly initialized.

- 2) The fitness of each particle is evaluated. The position and fitness of each particle are stored in the particle's p_{best} . For the particle with the best value of p_{best} in the entire particle swarm, the position and fitness function value of this particle are stored as the g_{best} .
- 3) According to equation (15), the position and velocity of each particle are updated.
- 4) The new fitness function value of each particle is evaluated. If the new fitness function value is better than the particle's p_{best} value, the particle's p_{best} value is updated with the current position and fitness function value.
- 5) For the particle swarm, the new g_{best} value is also obtained. If the fitness function value of the new g_{best} is better than the fitness function value of the existing g_{best} , the value of g_{best} is updated with the current position and fitness function value of new g_{best} .
- 6) The steps 3 to 5 are repeated until n reaches the maximum number of iterations or the preset position accuracy is met.

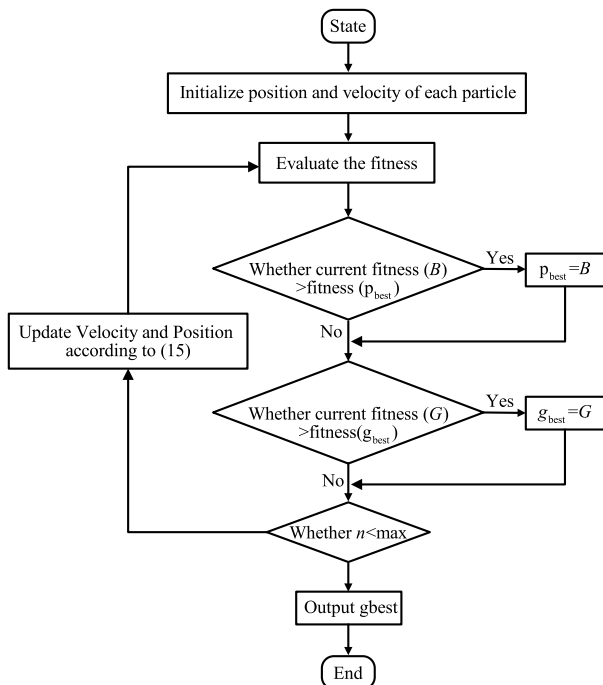


FIGURE 3. The flow chart of the PSO algorithm.

C. REDUCING THE NUMBER OF SENSORS

From Fig. 2, it should be noted that the PBC controller needs to sample the full status, including inverter-side current, capacitor voltage, grid-injected current and PCC voltage. The sampled state variables require many sensors, which increases system cost. In order to reduce the number of sensors, the use of a Kalman filter observer is proposed in this article to estimate the state variables. Only the grid-injected current is retained as a sampling signal, while inverter-side current, capacitor voltage and PCC voltage can be estimated by the Kalman filter observer.

In the Kalman filter algorithm, the state-space form of mathematical equation (1) is expressed as (17). Due to the symmetrical system structure, only the α -axis is shown. The state vector is redefined as $x = [i_{1\alpha} \ u_{c\alpha} \ i_{2\alpha} \ v_{pcc\alpha}^q \ v_{pcc\alpha}^q]$, where $v_{pcc\alpha}^q$ is the quadrature component of the voltage of $v_{pcc\alpha}$.

$$\begin{cases} \dot{x}_\alpha = Ax_\alpha + Bu_\alpha \\ y_\alpha = Cx_\alpha \end{cases} \quad (17)$$

where

$$A = \begin{bmatrix} -\frac{R_1}{L_1} & \frac{1}{L_1} & 0 & 0 & 0 \\ \frac{1}{C} & 0 & -\frac{1}{C} & 0 & 0 \\ 0 & \frac{1}{L_2} & -\frac{R_2}{L_2} & -\frac{1}{L_2} & 0 \\ 0 & 0 & 0 & 0 & \omega_g \\ 0 & 0 & 0 & -\omega_g & 0 \end{bmatrix},$$

$$B = \begin{bmatrix} \frac{1}{L_1} & 0 & 0 & 0 & 0 \end{bmatrix}^T,$$

$C = [0 \ 0 \ 1 \ 0 \ 0]$, $y_\alpha = i_{2\alpha}$ and ω_g is the grid angular frequency.

By discretizing the state-space equations (17), it can be obtained that

$$\begin{cases} x_\alpha(k+1) = A_1 x_\alpha(k) + B_1 u_\alpha(k) + \omega(k) \\ y_\alpha(k) = C x_\alpha(k) + v(k) \end{cases} \quad (18)$$

where $A_1 = e^{AT_s}$, $B_1 = \int_0^{T_s} e^{A\tau} d\tau B$, T_s is sample period, k is the discrete sampling instant. $\omega(k)$ and $v(k)$ are the process and measurement noise vectors, respectively.

The covariance matrices of $\omega(k)$ and $v(k)$ are expressed as

$$Q(k) = E[\omega(k)\omega(k)^T], \quad R(k) = E[v(k)v(k)^T]. \quad (19)$$

The error covariance matrix of $x_\alpha(k)$ are defined as $p_\alpha(k)$. In the current step, the first prediction value $\hat{x}_\alpha(k/k-1)$ of the state vector and its corresponding error covariance matrix $\hat{p}_\alpha(k/k-1)$ can be obtained by the previous prediction value, which are expressed as

$$\begin{cases} \hat{x}_\alpha(k/k-1) = A_1 \cdot \hat{x}_\alpha(k-1) + B_1 u_\alpha(k-1) \\ \hat{p}_\alpha(k/k-1) = A_1 \cdot \hat{p}_\alpha(k-1) \cdot A_1^T + Q(k). \end{cases} \quad (20)$$

Then, the final estimates $\hat{x}_\alpha(k)$ of the state vector and its corresponding error covariance matrix $\hat{p}_\alpha(k)$ can be determined as

$$\begin{cases} \hat{x}_\alpha(k) = \hat{x}_\alpha(k/k-1) + T(k) \cdot [y(k) - C \cdot \hat{x}_\alpha(k/k-1)] \\ \hat{p}_\alpha(k) = [I - T(k) \cdot C] \cdot \hat{p}_\alpha(k/k-1) \end{cases} \quad (21)$$

where $T(k)$, the Kalman filter gain, is calculated recursively to minimize the mean square error between the measured values and the predicted values [35], which is used to update the state vector and error covariance matrix at each time step. The Kalman filter gain is defined as

$$T(k) = \hat{p}_\alpha(k/k-1) \cdot C^T \cdot [C \cdot \hat{p}_\alpha(k/k-1) \cdot C^T + R(k)]^{-1} \quad (22)$$

In order to further understand the Kalman filter observer, the block diagram of the Kalman filter observer is shown in Fig. 4, where the covariance matrices Q and R are both determined as 0.1.

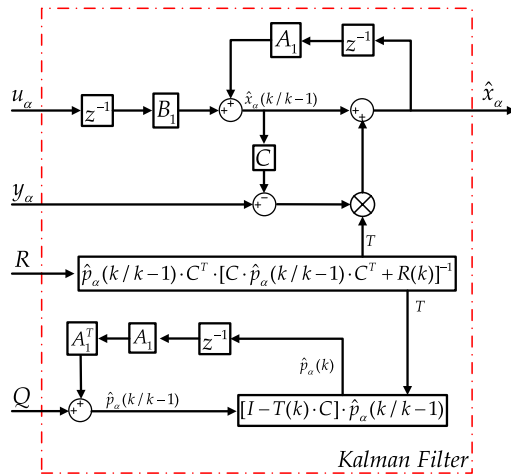


FIGURE 4. Schematic diagram of the Kalman filter observer.

IV. SIMULATION RESULTS

In order to verify the effectiveness of the proposed strategy, simulation tests on the GCI with an LCL filter are carried out in MATLAB/Simulink environment. The parameters of a 3-kW LCL-filtered GCI and the PSO algorithm are listed in Table 1.

TABLE 1. The parameters of the PSO algorithm.

Symbol	Description	Value
V_g	Grid voltage	110 V(RMS)
f, f_s	Switching and sampling frequency	10 kHz
U_{dc}	DC bus voltage	350 V
L_1	Inverter-side inductor	1.2 mH
C	Filter capacitor	6 μ F
L_2	Grid-side inductor	1.2 mH
$i_{2\alpha}^*$	Reference current	12.86 A (peak)
R_1, R_2	parasitic resistors	0.1 Ω
S	The number of particles	30
w	inertial weight	0.8
C_1, C_2	scaling factors	2
N	maximum iterations	50
k_p	range of k_p	[0,10]
k_r	range of k_r	[0,500]
r_2	range of r_2	[0,5]
r_3	range of r_3	[0,5]

A. PARAMETERS SELETED BY PSO ALGORITHM

According to the Fig. 3 and Table 1, simulation of the PSO algorithm is implemented to optimize the parameters k_p, k_r, r_2 and r_3 . During the optimization process, the

parameters of controller are updated in each iteration and the best parameters are selected based on the fitness function. The results of optimization parameters are shown in Fig. 5. It can be seen that the optimal parameters are: $k_p = 9.416$, $k_r = 467.882$, $r_2 = 0.021$, $r_3 = 0.577$.

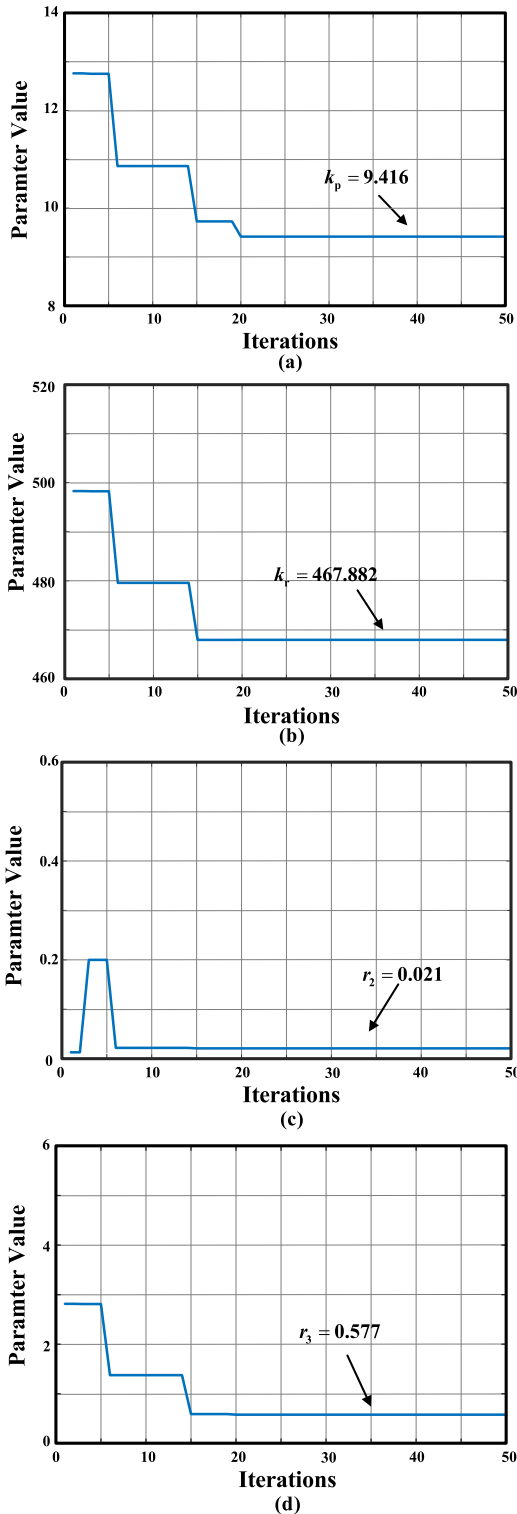


FIGURE 5. The results of optimization parameters: (a) k_p , (b) k_r , (c) r_2 , (d) r_3 .

B. ROBUSTNESS ANALYSIS AGAINST PARAMETERS SHIFT OF LCL FILTER

In order to verify the robustness of the PBC controller, the pole maps of the closed-loop transfer function G of the whole system is depicted in Fig. 6. Since the integral

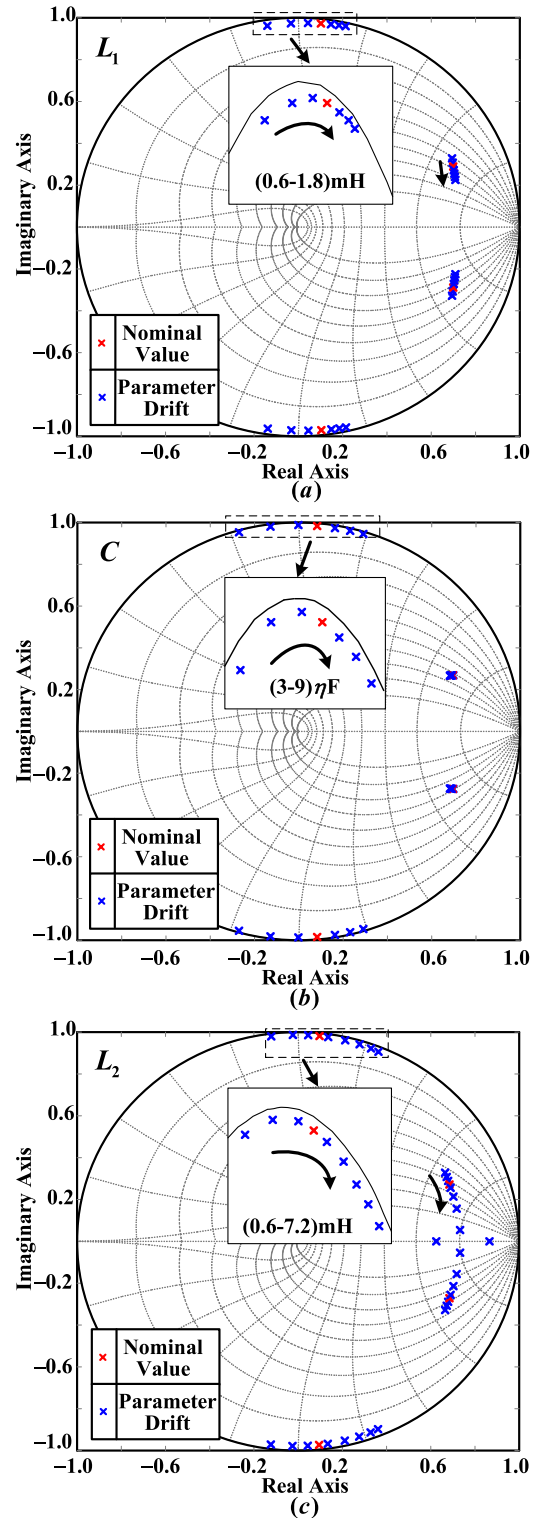


FIGURE 6. Pole maps of the closed-loop transfer function. (a) L_1 varies from 50% to 150%, (b) C varies from 50% to 150%, (c) L_2 varies from 50% to 500%.

TABLE 2. Cases at different rated power.

	Rated power	Switching frequency	Phase voltage	Reference current	L_1	C	L_2	k_p	k_r	r_2	r_3
Case 1	3kW	10 kHz	110 V(RMS)	12.86 A	1.2 mH	6 μ F	1.2 mH	9.416	467.882	0.021	0.577
Case 2	90 kW	8 kHz	220 V(RMS)	192 A	150 μ H	80 μ F	150 μ H	0.581	315.263	0.013	0.127
Case 3	300 kW	5 kHz	220 V(RMS)	643 A	60 μ H	300 μ F	60 μ H	0.214	153.954	0	0.013

coefficient k_r and parasitic resistors R have little effect on stability of system, they can be ignored to simplify the calculation. The detailed expressions of the closed-loop transfer function G can be found in the appendix. L_1 varies in the range of 0.6 mH-1.8 mH (50%~150% of L_1), C varies in the range of 3 μ F-9 μ F (50%~150% of C) and L_2 varies in the range of 0.6 mH-6 mH (50%~500% of L_2), respectively. In each case, only one parameter in the LCL filter varies. From Fig. 6, it can be seen that all closed-loop poles of system are located inside the unity circle, which means that the PBC controller using the parameters designed by PSO has strong robustness against parameters variation.

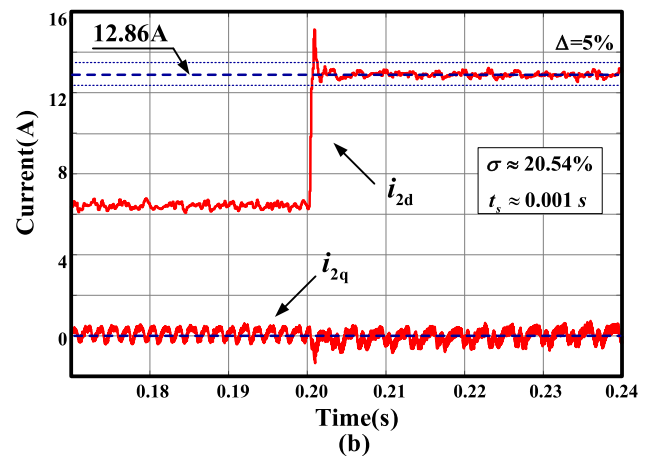
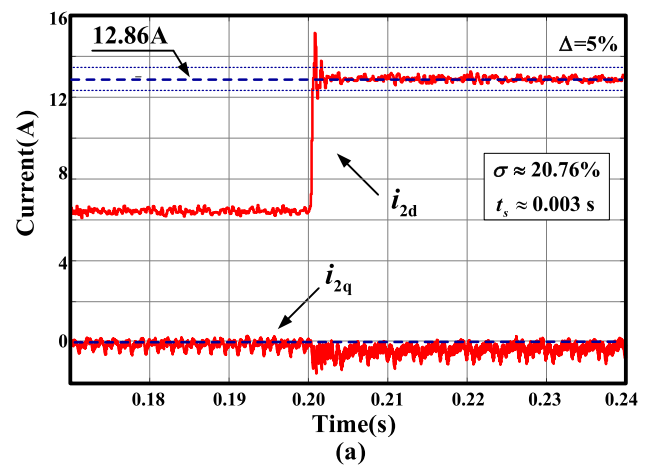
C. TRANSIENT RESPONSES UNDER THE STEP CHANGE

To verify the effectiveness of the parameters provided by PSO algorithm, the simulation of the proposed PBC controller is carried out. In addition, the parameters designed by [18] ($k_p = 8$, $k_i = 800$, $r_2 = 0.02$, $r_3 = 4$) is also used as a comparative experiment. Fig. 7 shows the transient responses of the grid-injected current controlled by the proposed PBC and conventional PBC on d-q axis, where the current reference starts from 6.43 A step to 12.86 A at $t = 0.20$ s.

It can be seen that the overshoot (σ) and settling time (t_s) of the conventional PBC are about 20.76 % and 0.002 s, respectively; the overshoot (σ) and settling time (t_s) of the proposed PBC are about 20.54 % and 0.001 s, respectively. Compared with the conventional PBC, the parameters of the PBC controller selected by PSO algorithm can achieve almost the same dynamic performance. This confirms that PSO algorithm is an effective method to design the parameters of the PBC controller.

D. STEADY-STATE WAVEFORMS AT DIFFERENT RATED POWER

This test is conducted to verify the steady-state performance of the grid-injected current under different rated power levels. Table 2 records the experimental conditions of three cases and corresponding controller parameters obtained by the PSO algorithm. The simulated results of the grid-injected current are shown in Fig. 8. It can be observed that the grid-injected currents remain sinusoidal waveforms with zero steady-state error, whose THDs are about 2.24%, 3.22%, 2.20%, respectively. This confirms that the grid-injected current can be well controlled by the proposed PBC controller at different rated power levels.

**FIGURE 7.** The transient responses of the grid-injected current controlled by (a) Conventional PBC and (b) Proposed PBC.

E. ESTIMATION EVALUATION OF KALMAN FILTER OBSERVER

This test is conducted to verify the performance of the Kalman filter observer. The inverter-side current i_1 , the capacitor voltage u_c and the PCC voltage v_{pcc} estimated by the Kalman filter observer, respectively, are shown in Fig. 9. In addition, to show the superior performances of the Kalman filter observer, the actual values are also measured and presented in Fig. 9.

From Fig. 9, it can be seen that the values estimated by the Kalman filter observer are almost the same as the measured

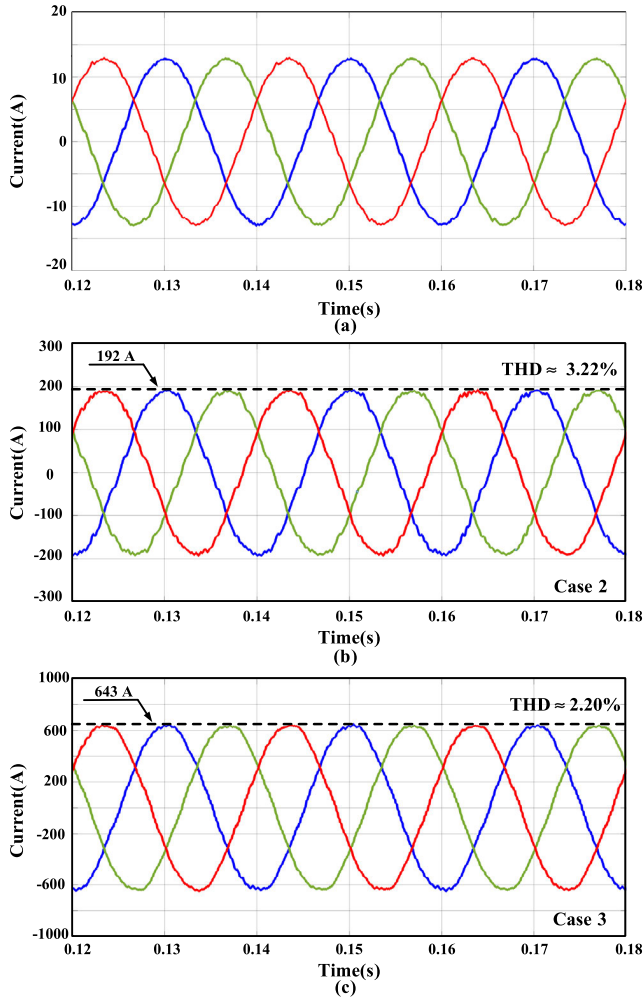


FIGURE 8. The grid-injected current under different rated power. (a) 3kW. (b) 90kW. (c) 300kW.

ones. Thus, the use of a Kalman filter observer is a feasible design method for the PBC controller.

V. EXPERIMENTAL VERIFICATIONS

In order to further verify the effectiveness of the proposed method, a 3kW/3-phase/110V grid-connected inverter setup was constructed for experiments, which is shown in Fig. 10. Chroma 62150H-600S DC power supply provide a dc-link voltage. The digital control algorithm is implemented in dSPACE 1202 microlabbox. The waveforms of grid voltage and grid-injected current were measured with a Yokogawa DL 1640 digital oscilloscope. The parameters of experiments are also listed in Table 1.

A. STEADY-STATE PERFORMANCE IN STIFF GRID

The experimental steady-state waveforms of the grid voltage and the grid-injected current under the condition of stiff grid ($L_g = 0$ mH) are depicted in Fig. 11. In addition, the conventional PBC in [18] was also implemented and tested as

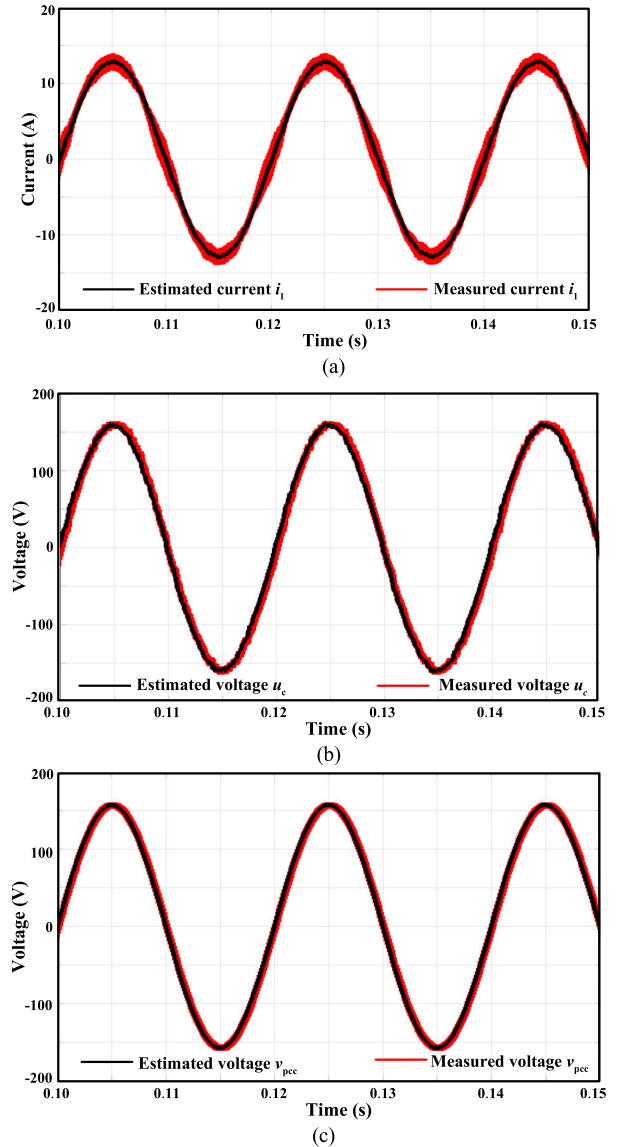


FIGURE 9. Comparison between the estimated values using Kalman filter observer and the measured ones: (a) the inverter-side current, (b) the capacitor voltage, (c) the PCC voltage.

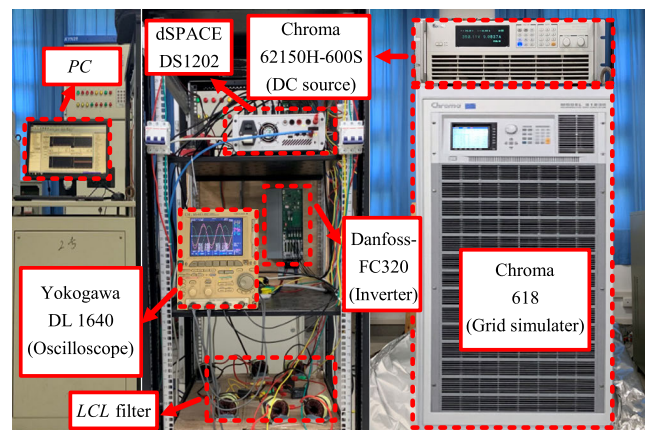


FIGURE 10. Experimental setup with a 3 kW/3-phase/110V GCI.

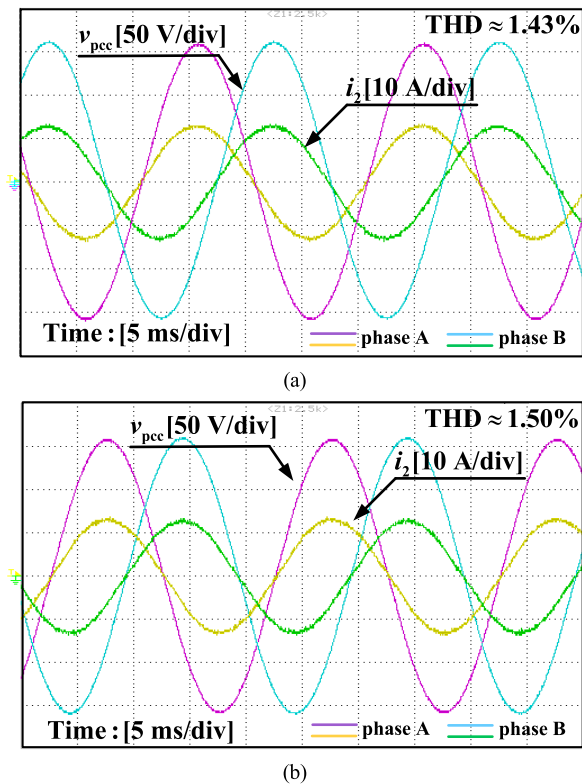


FIGURE 11. Experimental steady-state waveforms of the grid voltages and the grid-injected currents under $L_g = 0$ mH: (a) Proposed PBC. (b) Conventional PBC.

a comparative experiment. It can be seen that both of them can achieve unit power factor and zero steady-state error. The proposed PBC controller with Kalman filter observer can ensure the quality of the grid-injected current, where its total harmonics distortion (THD) is about 1.43%.

B. TRANSIENT RESPONSE IN WEAK GRID

In actual applications, the electric grid usually has an equivalent grid inductor, which may change in over a large range. To verify the transient response of the proposed control method in the presence of the grid inductance, the external inductors ($L_g = 4.8$ mH) were connected and the current reference value steps was reduced down from 12.86 A to 6.43 A. Fig. 12 shows the measured grid-injected currents of the proposed PBC and the conventional PBC, respectively, under the a weak grid condition. It can be seen that both of them are able to accurately track the reference current. The transient response, with a settling time of approximately 4 ms under proposed PBC is faster than that of conventional PBC. In addition, the oscillation under proposed PBC is smaller than conventional PBC. This demonstrates that the proposed PBC controller exhibits better transient performance against the grid impedance variations.

C. ROBUSTNESS TO THE PARAMETER VARIATION

The following experiment is performed to investigate the sensitivity of the grid-injected current against the parameter uncertainties. The inverter-side inductor L_1 decreases from

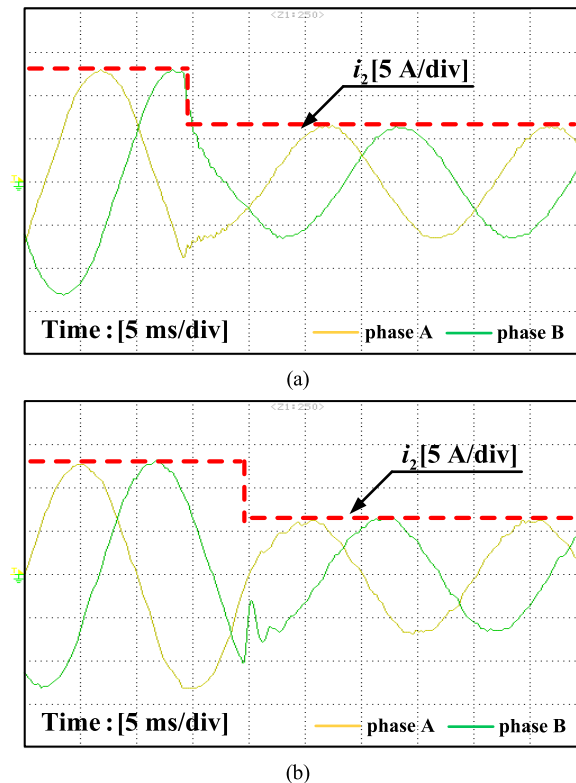


FIGURE 12. Experimental dynamic waveforms of the grid-injected current under $L_g = 4.8$ mH. (a) Proposed PBC. (b) Conventional PBC.

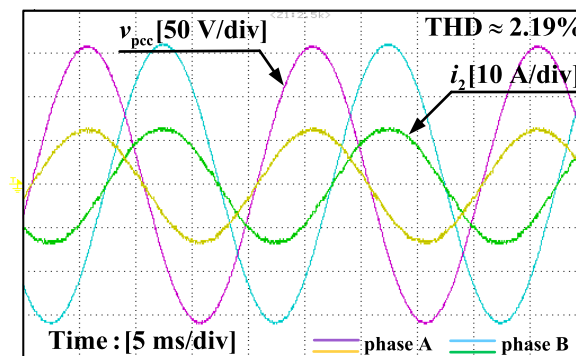


FIGURE 13. Experimental waveforms of the grid voltage and the grid-injected current under the parameter variation of -33.3% in L_1 , -5% in C and -33% in L_2 .

1.2 mH to 0.8 mH (33.3% dips), the grid-side inductor L_2 drops from 1.2 mH to 0.8 mH (33.3% dips), the filtering capacitor C reduces from 6 μ F to 5.7 μ F (5% dips), simultaneously. The experimental waveforms of the grid-injected current and grid voltage are shown in Fig. 13. It can be seen that the grid-injected current still be stable and achieve zero steady-state error, which means that the proposed PBC has strong robustness against the parameter variations.

D. ABILITY TO REJECT THE GRID DISTURBANCES

In practice, harmonic voltages often exist in the power grid, which will affect the waveform of the grid-injected current. In order to suppress them, the harmonics of the electric grid voltage are considered as extended state variables in the observer model according to [36], [37]. When the grid voltage is distorted by the 3rd, 5th, 7th harmonics, whose magnitudes with respect to the grid fundamental voltage are all 3%, the grid voltage and the grid-injected current under a weak grid condition ($L_g = 3.6$ mH) are shown in Fig. 14. It can be observed that the grid-injected current exhibits a good sinusoidal waveform and the harmonics of the grid voltage has been successfully attenuated.

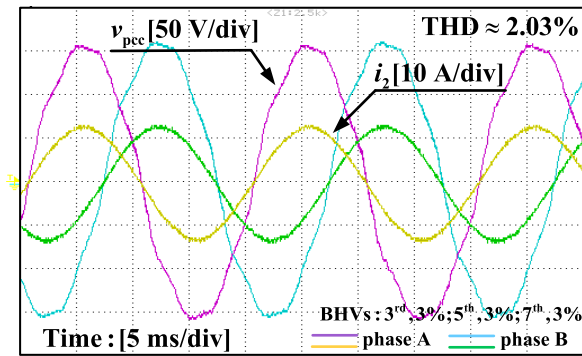


FIGURE 14. Experimental waveforms of the grid voltage and the grid-injected current under a distorted grid voltage and $L_g = 3.6$ mH.

In addition, to further prove the ability of the proposed PBC to reject the grid disturbances, the experimental steady-state waveform of the grid-injected current and the unbalanced grid voltage when the grid impedance L_g is 4.8 mH and the grid voltage is reduced by 25% in Phase A, are shown in Fig. 15.

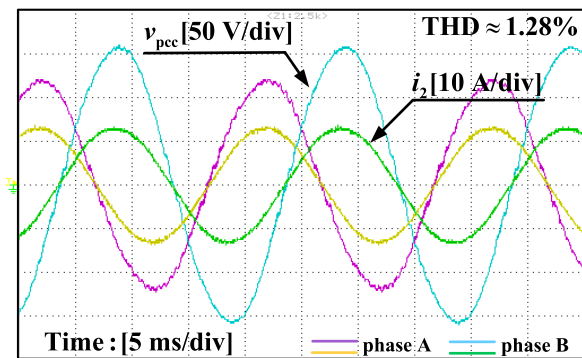


FIGURE 15. Experimental waveforms of the grid voltage and the grid-injected current under unbalanced grid voltage and $L_g = 4.8$ mH.

VI. CONCLUSION

In this article, the operating parameter values of the PBC controller of a three-phase LCL-filtered GCI are derived by applying the PSO algorithm. Moreover, a Kalman filter observer is adopted to effectively reduce the number of sensors. The conclusions can be summarized as follows:

- 1) The parameter values of a PBC controller (including a PR regulator) can be successfully obtained by applying the PSO algorithm, which is more convenient and easier to use than the method introduced in [18], especially for inexperienced engineers.
- 2) The proposed PBC controller only uses grid-injected current sensors and has slightly better control performance than the conventional one.
- 3) The proposed PBC still has also very strong robustness against the parameter variations and external disturbance.

All the analysis has been successfully verified through simulations and experiments on a 3-kW/50Hz/110V/three-phase laboratory setup.

APPENDIX

$$G(s) = \frac{i_{2\alpha}(s)}{i_{2\alpha}^*(s)} = \frac{T_d[a_0s^3 + a_1s^2 + a_2s + a_3]}{b_0s^3 + b_1s + T_d[c_0s^2 + c_1s + c_2]}$$

where

$$\begin{aligned} a_0 &= C_e L_1 L_2, & a_1 &= r_2 L_1 L_2 + r_3 C_e L_2 + k_p C_e L_1, \\ a_2 &= r_2 r_3 L_2 + k_p r_2 L_1 + k_p r_3 C_e + L_1 + L_2, \\ a_3 &= k_p r_2 r_3 + k_p + r_3, & b_0 &= C L_1 L_2, & b_1 &= L_1 + L_2, \\ c_0 &= k_p C_e L_1 + r_3 C L_2 + L_1 r_2 L_2, \\ c_1 &= k_p r_2 L_1 + k_p r_3 C_e + r_2 r_3 L_2, & c_2 &= k_p r_2 r_3 + k_p + r_3, \\ T_d &= e^{-1.5sT_s} \approx \frac{1}{1.5sT_s + 1}. \end{aligned}$$

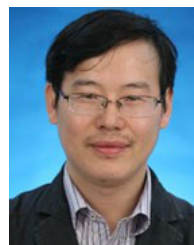
REFERENCES

- [1] S. Luo, F. Wu, and K. Zhao, "Modified single-carrier multilevel SPWM and online efficiency enhancement for single-phase asymmetrical NPC grid-connected inverter," *IEEE Trans. Ind. Informat.*, vol. 16, no. 5, pp. 3157–3167, May 2020.
- [2] Y. Guan, Y. Wang, Y. Xie, Y. Liang, A. Lin, and X. Wang, "The dual-current control strategy of grid-connected inverter with LCL filter," *IEEE Trans. Power Electron.*, vol. 34, no. 6, pp. 5940–5952, Jun. 2019.
- [3] T. Liu, J. Liu, Z. Liu, and Z. Liu, "A study of virtual resistor-based active damping alternatives for LCL resonance in grid-connected voltage source inverters," *IEEE Trans. Power Electron.*, vol. 35, no. 1, pp. 247–262, Jan. 2020.
- [4] J. Dannehl, F. W. Fuchs, S. Hansen, and P. B. Thøgersen, "Investigation of active damping approaches for PI-based current control of grid-connected pulse width modulation converters with LCL filters," *IEEE Trans. Ind. Appl.*, vol. 46, no. 4, pp. 1509–1517, Jul. 2010.
- [5] G. Shen, X. Zhu, J. Zhang, and D. Xu, "A new feedback method for PR current control of LCL-Filter-Based grid-connected inverter," *IEEE Trans. Ind. Electron.*, vol. 57, no. 6, pp. 2033–2041, Jun. 2010.
- [6] R. A. Fantino, C. A. Busada, and J. A. Solsona, "Optimum PR control applied to LCL filters with low resonance frequency," *IEEE Trans. Power Electron.*, vol. 33, no. 1, pp. 793–801, Jan. 2018.
- [7] W. Wu, Y. Liu, Y. He, H. S. H. Chung, M. Liserre, and F. Blaabjerg, "Damping methods for resonances caused by LCL-filter-based current-controlled grid-tied power inverters: An overview," *IEEE Trans. Ind. Electron.*, vol. 64, no. 9, pp. 7402–7413, Sep. 2017.
- [8] R. Peña-Alzola, M. Liserre, F. Blaabjerg, R. Sebastián, J. Dannehl, and F. W. Fuchs, "Analysis of the passive damping losses in LCL-filter-based grid converters," *IEEE Trans. Power Electron.*, vol. 28, no. 6, pp. 2642–2646, Jun. 2013.
- [9] C. Bao, X. Ruan, X. Wang, W. Li, D. Pan, and K. Weng, "Step-by-step controller design for LCL-type grid-connected inverter with capacitor-current-feedback active-damping," *IEEE Trans. Power Electron.*, vol. 29, no. 3, pp. 1239–1253, Mar. 2014.

- [10] M. G. Judewicz, S. A. Gonzalez, J. R. Fischer, J. F. Martinez, and D. O. Carrica, "Inverter-side current control of grid-connected voltage source inverters with LCL filter based on generalized predictive control," *IEEE J. Emerg. Sel. Topics Power Electron.*, vol. 6, no. 4, pp. 1732–1743, Dec. 2018.
- [11] S. Bosch, J. Staiger, and H. Steinhart, "Predictive current control for an active power filter with LCL-filter," *IEEE Trans. Ind. Electron.*, vol. 65, no. 6, pp. 4943–4952, Jun. 2018.
- [12] J. Scoltock, T. Geyer, and U. K. Madawala, "A model predictive direct current control strategy with predictive references for MV grid-connected converters with LCL-filters," *IEEE Trans. Power Electron.*, vol. 30, no. 10, pp. 5926–5937, Oct. 2015.
- [13] R. P. Vieira, L. T. Martins, J. R. Massing, and M. Stefanello, "Sliding mode controller in a multiloop framework for a grid-connected VSI with LCL filter," *IEEE Trans. Ind. Electron.*, vol. 65, no. 6, pp. 4714–4723, Jun. 2018.
- [14] N. Altin, S. Ozdemir, H. Komurcugil, and I. Sefa, "Sliding-mode control in natural frame with reduced number of sensors for three-phase grid-tied LCL-interfaced inverters," *IEEE Trans. Ind. Electron.*, vol. 66, no. 4, pp. 2903–2913, Apr. 2019.
- [15] M. Merai, M. W. Naouar, I. Slama-Belkhdja, and E. Monmasson, "An adaptive PI controller design for DC-link voltage control of single-phase grid-connected converters," *IEEE Trans. Ind. Electron.*, vol. 66, no. 8, pp. 6241–6249, Aug. 2019.
- [16] Z.-X. Zou, G. Buticchi, and M. Liserre, "Grid identification and adaptive voltage control in a smart transformer-fed grid," *IEEE Trans. Power Electron.*, vol. 34, no. 3, pp. 2327–2338, Mar. 2019.
- [17] J. Li, X. Lv, B. Zhao, Y. Zhang, Q. Zhang, and J. Wang, "Research on passivity based control strategy of power conversion system used in the energy storage system," *IET Power Electron.*, vol. 12, no. 3, pp. 392–399, Mar. 2019.
- [18] J. Zhao, W. Wu, Z. Shuai, A. Luo, H. S.-H. Chung, and F. Blaabjerg, "Robust control parameters design of PBC controller for LCL-filtered grid-tied inverter," *IEEE Trans. Power Electron.*, vol. 35, no. 8, pp. 8102–8115, Aug. 2020.
- [19] R. Ortega, A. van der Schaft, F. Castanos, and A. Astolfi, "Control by interconnection and standard passivity-based control of port-Hamiltonian systems," *IEEE Trans. Autom. Control*, vol. 53, no. 11, pp. 2527–2542, Dec. 2008.
- [20] X. Wang, F. Blaabjerg, and P. C. Loh, "Passivity-based stability analysis and damping injection for multiparalleled VSCs with LCL filters," *IEEE Trans. Power Electron.*, vol. 32, no. 11, pp. 8922–8935, Nov. 2017.
- [21] J. Lai, X. Yin, E. Lei, Y. Chen, and X. Yin, "Passivity control based on Euler-Lagrangian model for D-STATCOM with LCL filter," in *Proc. 12th World Congr. Intell. Control Automat. (WCICA)*, Guilin, China, Jun. 2016, pp. 1561–1565.
- [22] M. A. Hassan and M. A. Abido, "Optimal design of microgrids in autonomous and grid-connected modes using particle swarm optimization," *IEEE Trans. Power Electron.*, vol. 26, no. 3, pp. 755–769, Mar. 2011.
- [23] B. Ufnalski, A. Kaszewski, and L. M. Grzesiak, "Particle swarm optimization of the multioscillatory LQR for a three-phase four-wire voltage-source inverter with an LC output filter," *IEEE Trans. Ind. Electron.*, vol. 62, no. 1, pp. 484–493, Jan. 2015.
- [24] C. A. C. Coello, G. T. Pulido, and M. S. Lechuga, "Handling multiple objectives with particle swarm optimization," *IEEE Trans. Evol. Comput.*, vol. 8, no. 3, pp. 256–279, Jun. 2004.
- [25] C. A. Busada, S. Gomez Jorge, and J. A. Solsona, "Full-state feedback equivalent controller for active damping in LCL-filtered grid-connected inverters using a reduced number of sensors," *IEEE Trans. Ind. Electron.*, vol. 62, no. 10, pp. 5993–6002, Oct. 2015.
- [26] J. Kukkola and M. Hinkkanen, "Observer-based state-space current control for a three-phase grid-connected converter equipped with a LCL filter," *IEEE Trans. Ind. Appl.*, vol. 50, no. 4, pp. 2700–2709, Jul. 2014.
- [27] B. Bolsens, K. D. Brabandere, J. V. Den Keybus, J. Driesen, and R. Belmans, "Model-based generation of low distortion currents in grid-coupled PWM-inverters using an LCL output filter," *IEEE Trans. Power Electron.*, vol. 21, no. 4, pp. 1032–1040, Jul. 2006.
- [28] Q. Qian, S. Xie, J. Xu, K. Xu, S. Bian, and N. Zhong, "Output impedance modeling of single-phase grid-tied inverters with capturing the frequency-coupling effect of PLL," *IEEE Trans. Power Electron.*, vol. 35, no. 5, pp. 5479–5495, May 2020.
- [29] R. Ortega, A. Loria, P. J. Nicklasson, and H. Sira-Ramirez, *Passivity-Based Control of Euler-Lagrange Systems*. Berlin, Germany: Springer-Verlag, 1998.
- [30] Y. Gupta, K. Chatterjee, and S. Doolla, "Controller design, analysis and testing of a three-phase VSI using IDA–PBC approach," *IET Power Electron.*, vol. 13, no. 2, pp. 346–355, Feb. 2020.
- [31] J. Lai, X. Yin, L. Jiang, X. Yin, Z. Wang, and Z. Ullah, "Disturbance-Observed-Based PBC for static synchronous compensator under system disturbances," *IEEE Trans. Power Electron.*, vol. 34, no. 11, pp. 11467–11481, Nov. 2019.
- [32] G. Bergna-Diaz, D. Zonetti, S. Sanchez, R. Ortega, and E. Tedeschi, "PI passivity-based control and performance analysis of MMC multiterminal HVDC systems," *IEEE J. Emerg. Sel. Topics Power Electron.*, vol. 7, no. 4, pp. 2453–2466, Dec. 2019.
- [33] L. Guihua, W. Wenxiu, Z. Xiaohui, and W. Wei, "Improved Passivity-Based Control Method of Grid-Connected PV Inverter in Weak Grids," in *Proc. 21st Int. Conf. Elect. Mach. Syst. (ICEMS)*, Jeju, South Korea, Oct. 2018, pp. 1151–1156.
- [34] Y. Liu, W. Wu, Y. He, Z. Lin, F. Blaabjerg, and H. S.-H. Chung, "An efficient and robust hybrid damper for LCL-or LLCL-based grid-tied inverter with strong grid-side harmonic voltage effect rejection," *IEEE Trans. Ind. Electron.*, vol. 63, no. 2, pp. 926–936, Feb. 2016.
- [35] M. Parvez, M. F. M. Elias, N. A. Rahim, F. Blaabjerg, D. Abbott, and S. F. Al-Sarawi, "Comparative study of discrete PI and PR controls for single-phase UPS inverter," *IEEE Access*, vol. 8, pp. 45584–45595, 2020.
- [36] K. H. Ahmed, A. M. Massoud, S. J. Finney, and B. W. Williams, "Sensorless current control of three-phase inverter-based distributed generation," *IEEE Trans. Power Del.*, vol. 24, no. 2, pp. 919–929, Apr. 2009.
- [37] M. Su, B. Cheng, Y. Sun, Z. Tang, B. Guo, Y. Yang, F. Blaabjerg, and H. Wang, "Single-sensor control of LCL-filtered grid-connected inverters," *IEEE Access*, vol. 7, pp. 38481–38494, 2019.



FABAN ZHENG was born in Zhejiang, China, in 1995. He received the B.S. degree in ship electrical engineering and electronic engineering from Shanghai Maritime University, Shanghai, China, in 2018, where he is currently pursuing the M.S. degree in electrical engineering. His current research interests include digital control techniques for power converters and renewable energy generation systems.



WEIMIN WU (Member, IEEE) received the Ph.D. degree in electrical engineering from the College of Electrical Engineering, Zhejiang University, Hangzhou, China, in 2005.

He worked as a Research Engineer at the Delta Power Electronic Center (DPEC), Shanghai, from July 2005 to June 2006. Since July 2006, he has been a Faculty Member with Shanghai Maritime University, where he is currently a Full Professor with the Department of Electrical Engineering.

He was a Visiting Professor with the Center for Power Electronics Systems (CPES), Virginia Polytechnic Institute and State University, Blacksburg, VA, USA, from September 2008 to March 2009. From November 2011 to January 2014, he was also a Visiting Professor with the Department of Energy Technology, Aalborg University, Denmark, working at the Center of Reliable Power Electronics (CORPE). He has coauthored over 100 articles and holds eight patents. His research interests include power converters for renewable energy systems, power quality, smart grid, and energy storage technology. He serves as an Associate Editor for the IEEE TRANSACTIONS ON INDUSTRIAL ELECTRONICS.



BOLIN CHEN (Member, IEEE) was born in Zhejiang, China, in 1997. He received the B.S. degree in electrical engineering from Shanghai Maritime University, Shanghai, China, in 2019, where he is currently pursuing the M.S. degree in electrical engineering. His current research interests include sliding mode control, digital control techniques, and renewable energy generation systems.



EFTICHIOS KOUTROULIS (Senior Member, IEEE) was born in Chania, Greece, in 1973. He received the Diploma, M.Sc., and Ph.D. degrees in electronic and computer engineering from the Technical University of Crete, in 1996, 1999, and 2002, respectively. In September 2002 he has served at the Department of Electronic and Computer Engineering, Technical University of Crete. He worked as a Visiting Researcher at the Department of Energy Technology, Aalborg University, Aalborg, Denmark. Since January 2012, he has been an Assistant Professor with the Department of Electronic and Computer Engineering, Technical University of Crete. His research interests include the design of power converters and microelectronic energy management systems for renewable energy sources applications and the design optimization of photovoltaic power plants. Since April 2011, he has been serving as a member of the Editorial Board of the *Renewable Energy Journal*.

• • •